Check for updates

# SiO$_2$@MnO$_x$@Na$_2$WO$_4$@SiO$_2$ core–shell-derived catalyst for oxidative coupling of methane†

La-Hee Park,[ab] Ye Rim Jo, [ID][a] Jae-Wook Choi,[a] Dong Jin Suh,[ab] Kwang Ho Song [ID][bc] and Jeong-Myeong Ha [ID] *[abd]

SiO$_2$@MnO$_x$@Na$_2$WO$_4$@SiO$_2$ core–shell catalysts were prepared and their fabrication was confirmed using transmission electron microscopy. The formation of Mn-based nanosheets on the silica spheres is important for the deposition of nanoscopic Na$_2$WO$_4$. The SiO$_2$@MnO$_x$@Na$_2$WO$_4$@SiO$_2$ core–shell catalysts were used for the oxidative coupling of methane at a temperature of 700–800 °C at which the nanostructures were completely destroyed. Although the core–shell structures did not survive the high-temperature oxidative coupling of methane, the selective production of olefins and paraffins can be attributed to highly dispersed Na$_2$WO$_4$ derived from confined core–shell structures.
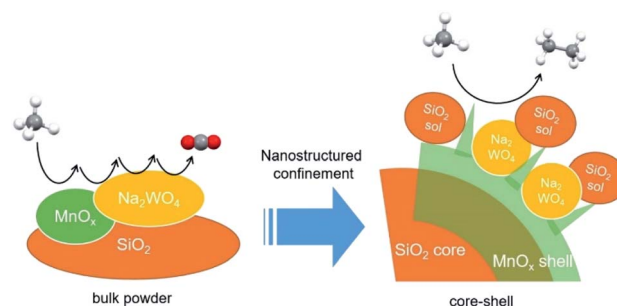
## 1. Introduction

Methane is a major component of natural gas and potential feedstock for the production of chemicals and fuels.[1,2] While it is a building block for the preparation of many complex organic chemicals, the conversion of stable C–H bonds is difficult. Methane can be indirectly transformed into larger organic molecules via synthesis gas.[3] It can also be directly converted into functionalized building blocks including methanol,[4] methyl halides,[5] and ethylene.[6] Oxidative coupling of methane (OCM) to paraffins and olefins has attracted much interest because of its high productivity.[3,7,8] Because catalysts are important for the determination of the efficiency of OCM, many catalysts have been suggested for the development of economically feasible processes.[7,9,10]

Several metal oxide catalysts including perovskites,[11,12] metal oxide nanoparticles,[13] and other mixed metal oxides[14] have been proposed for the active and selective OCM process. One of the most efficient OCM catalysts,[15] Na$_2$WO$_4$/Mn/SiO$_2$ can be fabricated by depositing Na$_2$WO$_4$ and Mn on an SiO$_2$ support. Although the reaction mechanism is still controversial,[9] it has been suggested that Na$_2$WO$_4$ and Mn act as active component and promoter, respectively.[9,16,17] Scientists attempted to improve the Na$_2$WO$_4$/Mn/SiO$_2$ catalyst by adding promoters[16,18,19] and modifying the support,[20] but nanostructured Na$_2$WO$_4$/Mn/SiO$_2$ has not been used because of the high OCM reaction temperature.

In this study, core–shell structures composed of Na$_2$WO$_4$–Mn–SiO$_2$ were prepared as precursors of OCM catalysts (Scheme 1). Based on the active or selective catalysis using core–shell structures reported in the literature,[21,22] the objectives of building a core–shell structure are the (i) dispersion of Na$_2$WO$_4$ and Mn on the silica surface, (ii) stabilization of Na$_2$WO$_4$ and Mn components at the high reaction temperatures of 700–900 °C, and (iii) formation of possible Na$_2$WO$_4$, Mn, and SiO$_2$ complexes to achieve an improved catalytic activity. Particularly, an outer shell of SiO$_2$ was added to immobilize Na$_2$WO$_4$ and MnO$_x$ shells at the high reaction temperature and to potentially prepare a highly dispersed mixture of Na$_2$WO$_4$, MnO$_x$, and silica which could improve the catalytic activity. By using the highly dispersed Na$_2$WO$_4$ of the core–shell precursors, the selective formation of ethane and ethylene is favored compared with the bulk Na$_2$WO$_4$/Mn/SiO$_2$ catalyst, which allows the deep oxidation to CO$_2$. While well-defined core–shell structures cannot survive

[a]Clean Energy Research Center, Korea Institute of Science and Technology, Seoul 02792, Republic of Korea. E-mail: jmha@kist.re.kr

[b]Graduate School of Energy and Environment (Green School), Korea University, Seoul 02841, Republic of Korea

[c]Department of Chemical and Biological Engineering, Korea University, Seoul 02841, Republic of Korea

[d]Division of Energy and Environment Technology, KIST School, Korea University of Science and Technology, Seoul 02792, Republic of Korea

† Electronic supplementary information (ESI) available. See DOI: 10.1039/d0ra05081d

Scheme 1 Methane activation using core–shell catalysts.

at high OCM reaction temperatures, they control the final annealed structures and thus potentially the OCM activity and selectivity. Active OCM components that are nano-confined by the initial core–shell structures can be prepared. The step-by-step preparation of core–shell particles and improvement of the OCM activity are discussed in this paper.

## 2. Methods

### 2.1. Materials

All chemicals were used without further purification. Sodium tungstate dihydrate ($Na_2WO_4 \cdot 2H_2O$) was purchased from Yakuri Pure Chemicals (Kyoto, Japan). Potassium permanganate ($KMnO_4$, 99.3%) was purchased from Daejung Co., Ltd. (Siheung, Korea). Manganese acetate tetrahydrate [$Mn(CH_3CO)_2 \cdot 4H_2O$, 99.99%] was purchased from Sigma-Aldrich (St. Louis, Missouri, USA). Silica gel ($SiO_2$, 70–230 mesh, 99.5%) was purchased from Alfa Aesar (Haverhill, Massachusetts, USA). The TEOS [$Si(OC_2H_5)_4$] was purchased from Sigma-Aldrich (St. Louis, Missouri, USA). Aqueous ammonia solution ($NH_3$ (aq), 28.0–30.0%) was purchased from Sigma-Aldrich (St. Louis, Missouri, USA). Methane (99.5%), oxygen (99.95%), and nitrogen (99.9%) were purchased from Shinyang Sanso (Seoul, Korea). Deionized (DI) water (18.2 MΩ m) was prepared using an aquaMAX-Ultra 370 series water purification system (Young Lin Instruments, Anyang, Korea).

### 2.2. Preparation of supported powder catalysts

The mixed slurry method was used to prepare $Na_2WO_4/Mn/SiO_2$ catalysts with 5 wt% $Na_2WO_4$ and 2 wt% Mn supported by $SiO_2$.[23] A silica gel support (28 g) was mixed with DI water (150 mL) and stirred at 105 °C for 1 h. The $Mn(NO_3)_2 \cdot 6H_2O$ (1.8 mL) dissolved in DI water (10 mL) and $Na_2WO_4 \cdot 2H_2O$ (1.684 g) dissolved in DI water (10 mL) were drop-wise added to the boiling mixture for 15 min using a syringe pump. The generated thick paste was dried in air at 105 °C for 16 h and then calcined in air at 800 °C for 5 h. Prior to the reaction, the catalyst powder was sieved using a 150–250 mesh. Using the same procedure, additional catalysts were prepared by adding $KMnO_4$ or $Mn(CH_3CO)_2 \cdot 4H_2O$.

### 2.3. Preparation of $SiO_2$ spheres

The silica spheres used as cores were prepared using the Stöber method.[24–26] For this purpose, TEOS (30 mL) was hydrolysed in ethanol (170 mL) in the presence of aqueous ammonia solution (190 mL) and DI water (10 mL). The solvent was uniformly mixed using an impeller and added using a separatory funnel to hydrolyse the TEOS at a constant rate. The obtained silica spheres were washed with DI water and ethanol, centrifuged in a suspension, and dried in an oven at 80 °C for 24 h.

### 2.4. Preparation of $SiO_2@MnO_x$

The Mn species were deposited on the silica spheres ($SiO_2@MnO_x$) using a hydrothermal method. To prepare $SiO_2@Mn_xO_y$, the silica spheres (0.3 g) were dispersed in DI water (20 mL) at 30 °C for 1 h using ultrasonication,[27] followed by the addition of $KMnO_4$ (0.015–1.8 g) or $Mn(CH_3CO)_2 \cdot 4H_2O$ (or Mn-acetate, 0.15–1.8 g). Subsequently, the suspension was transferred to a Teflon-lined stainless-steel autoclave-type reactor and heated to 150 °C at a heating rate of 10 °C min$^{-1}$; the temperature was maintained at 150 °C for 48 h.[28–30] The autoclave-type reactor was then cooled to room temperature under ambient conditions. Subsequently, the $SiO_2@MnO_x(KMnO_4)$ and $SiO_2@MnO_x(Mn-acetate)$ core–shell structures were collected by centrifugation and washed five times or more with ethanol and DI water. Potassium ions were removed by washing the core–shell structures.

### 2.5. Preparation of $SiO_2@MnO_x@Na_2WO_4$

The $Na_2WO_4$ was deposited on $SiO_2@MnO_x$ by drying an aqueous $Na_2WO_4$ solution in an oil bath. The $Na_2WO_4 \cdot 2H_2O$ (0.012 g) dissolved in DI water (15 mL) was stirred for 30 min at room temperature. The $SiO_2@MnO_x$ (0.2 g) was added to the mixture, which then was stirred for an hour. The suspension was transferred to an oil bath preheated to 105 °C and stirred until the water solvent was completely evaporated. The prepared powder was dried in air at 80 °C for 6 h to completely remove any moisture.

### 2.6. Preparation of $SiO_2@MnO_x@Na_2WO_4@SiO_2$ core–shell structures

Nanostructured core–shell catalysts with three shell layers composed of the active components of the OCM catalyst were synthesized. First, the TEOS was hydrolysed using the Stöber method to fabricate silica spheres with sizes between 600–800 nm, which were used as cores. Subsequently, two manganese precursors were selected, and the silica spheres were coated with the $MnO_x$ shells using hydrothermal synthesis in a Teflon-lined stainless-steel autoclave. To attach $Na_2WO_4$ to the surface of the prepared $SiO_2@MnO_x$, DI water, $Na_2WO_4 \cdot 2H_2O$, and $SiO_2@MnO_x$ were added, followed by heating and stirring. Finally, the same method was used to fabricate silica spheres for the silica coating on the outermost layer of the catalyst.

### 2.7. Characterization of nanomaterials

Scanning electron microscopy (SEM) images of the catalysts were obtained using a Nova Nano SEM 200 instrument (FEI, Hillsboro, Oregon, USA). High-angle annular dark-field scanning transmission electron microscopy (HAADF-STEM) images of the catalysts were obtained using a Talos F200X instrument (FEI, Hillsboro, Oregon, USA). Both analyses were performed at the Korea Institute of Science and Technology (KIST) Advanced Analysis Center (Seoul, Korea). XRD results were collected using a Shimadzu XRD-6000 device equipped with a CuKα$_1$ ($\lambda$ = 0.15406 nm) source.

### 2.8. Catalytic activity measurement

The catalytic reaction was performed in a fixed bed reactor. The outlets and inlets of the quartz reactor had the same size (internal diameter = 6 mm, external diameter = 8 mm). The catalyst bed was in the center of the reactor and the quartz wool was placed in the upper and lower layers of the catalyst bed. To minimize any homogeneous reactions, $ZrSiO_4$ beads (Cenotec, Co., Ltd.) were

added to the quartz reactor. The $CH_4$ and $O_2$ reactants diluted with $N_2$, flowed to the catalyst bed with each gas flow was controlled by a mass flow controller (MFC). The catalyst bed was primed with a $N_2$ flow for 30 min prior to the reaction. Water produced during the OCM reaction was removed using a cold trap connected to a $-2\,°C$ chiller (Jeio Tech, VTRC-620) and the $CH_4$, $O_2$, $N_2$, CO, $CO_2$, and hydrocarbons were analysed using the methanizer-equipped-flame ionization detector (FID), thermal conductivity detector (TCD) and FID of online gas chromatograph (GC, Agilent 7890A with ShinCarbon ST GC Columns (micropacked, RESTEK, 100/120 mesh, 2 m, 80 psi) was used to detect hydrocarbons. The catalysis results were calculated as follows:

$$C_{2+} \text{ selectivity } (\%) = \frac{2 \times \text{moles of ethane and ethylene} + 3 \times \text{moles of propane and propylene}}{\text{moles of } CH_4 \text{ consumed}} \times 100$$

$$C_{2+} \text{ yield } (\%) = \frac{2 \times \text{moles of ethane and ethylene} + 3 \times \text{moles of propane and propylene}}{\text{moles of } CH_4 \text{ in the feed}} \times 100$$

$$CH_4 \text{ conversion } (\%) = \frac{\text{moles of } CH_4 \text{ consumed}}{\text{moles of } CH_4 \text{ in the feed}} \times 100$$

The standard deviations of measured $CH_4$ conversion and $C_{2+}$ selectivity were less than 5 and 3%, respectively.

## 3. Results and discussion

### 3.1. Preparation of $SiO_2$@$MnO_x$ particles

Prior to the fabrication of core–shell particles, silica spheres with diameters of 600–800 nm (Fig. 1) were prepared using the Stöber method.[24–26] The $SiO_2$@$MnO_x$ (Mn oxide shell deposited on $SiO_2$ spheres) was prepared by the deposition of $MnO_x$ on the

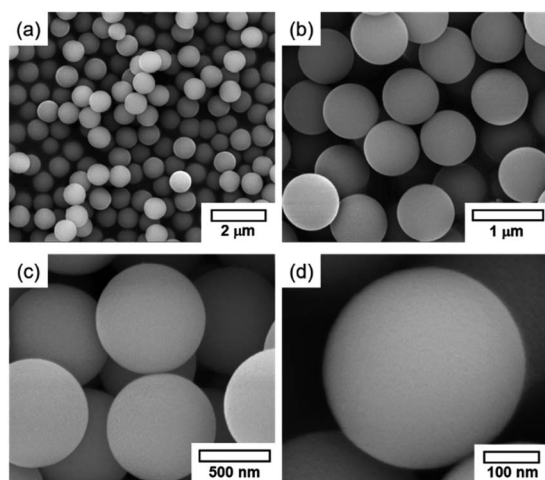cores of the silica spheres. The $MnO_x$ was deposited with a hydrothermal method utilizing $KMnO_4$ and $Mn(CH_3CO)_2$-$\cdot H_2O$ (Mn-acetate) as Mn species precursors.[28,29] The morphologies of the Mn shells differ depending on the Mn precursors. When $KMnO_4$ was used, plate-like shells formed on the surfaces of silica spheres. The morphology depends on the concentration of $KMnO_4$; the $(KMnO_4)/(SiO_2)$ ratio ranged from 0.02 to 2.22 (mol/mol). At a $(KMnO_4)/(SiO_2)$ ratio of 0.02–0.76 (mol/mol), $SiO_2$, the spheres were not completely covered with Mn species. However, they were completely covered at a $(KMnO_4)/(SiO_2)$ ratio of 1.52 (mol/mol) or higher. The Mn species, which completely cover the $SiO_2$ spheres, form nanoplate-like structures with a complex morphology that are stacked on top of each other (Fig. 2(f–h)). The transmission electron microscopy (TEM) images and energy dispersive X-ray spectroscopy (EDS) maps of $SiO_2$@$MnO_x$($KMnO_4$) confirm the deposition of nanoplate-like Mn species on the $SiO_2$ spheres and formation of Mn shells on $SiO_2$ spheres (Fig. 2(i–l)), respectively.

In addition to KMnO4, Mn-acetate was added to the silica spheres. The Mn-acetate forms shells on the silica spheres and Mn oxide nanowires (not deposited on the silica surface; Fig. 3(a–f)). Interestingly, the EDS maps indicate the formation of yolk–shell-like structures, creating empty space between the $MnO_x$ shells and silica spheres (Fig. 3(g and h)).

### 3.2. Preparation of $SiO_2$@$MnO_x$@$Na_2WO_4$

The $Na_2WO_4$ was added to $SiO_2$@$MnO_x$($KMnO_4$) and $SiO_2$@$MnO_x$(Mn-acetate). The deposition of $Na_2WO_4$ was analysed using EDS maps (Fig. 4). The morphology of $SiO_2$@$MnO_x$@$Na_2WO_4$ insignificantly differs from that of $SiO_2$@$MnO_x$. These observations indicate the $Na_2WO_4$ deposition in the empty space between the $MnO_x$ nanosheets and stabilization of $Na_2WO_4$ by $MnO_x$ shells. The roughness of the $MnO_x$ shells improves the deposition of $Na_2WO_4$ (Fig. 2 and 3). Note that $Na_2WO_4$ could not be deposited on the silica spheres without Mn species when a mixture of aqueous $Na_2WO_4$ solution and silica spheres was used, which indicates that it is difficult to deposit $Na_2WO_4$ on the silica surface and that an interaction between $Na_2WO_4$ and $MnO_x$ is required for the formation of a $Na_2WO_4$ layer.

### 3.3. Preparation of $SiO_2$@$MnO_x$@$Na_2WO_4$@$SiO_2$

The $SiO_2$@$MnO_x$@$Na_2WO_4$@$SiO_2$ core–shell catalyst was prepared by forming a silica shell on $SiO_2$@$MnO_x$@$Na_2WO_4$



Fig. 1 SEM images of silica spheres prepared using the Stöber method.
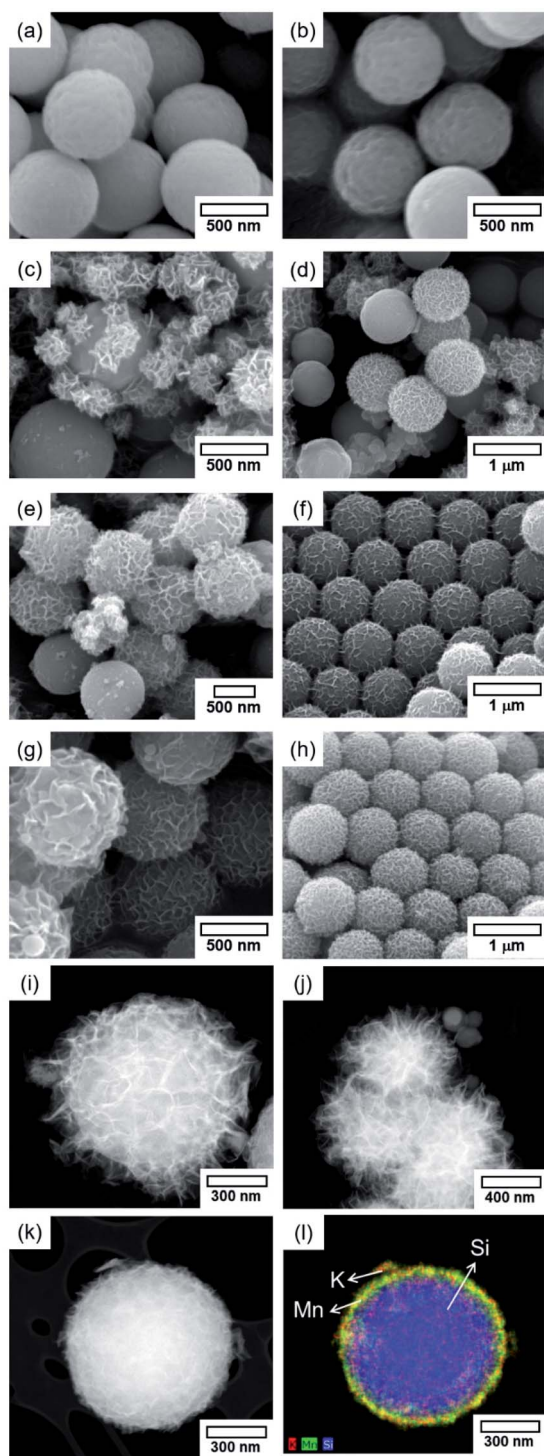
Fig. 2 SEM images of SiO$_2$@MnO$_x$(KMnO$_4$) with (KMnO$_4$)/(SiO$_2$) ratios of of (a) 0.02, (b) 0.04, (c) 0.38, (d) 0.57, (e) 0.76, (f) 1.52, (g) 1.90, and (h) 2.22 (mol/mol). (i and j) HAADF-STEM images of SiO$_2$@MnO$_x$(KMnO$_4$) with a (KMnO$_4$)/(SiO$_2$) ratio of 2.22 (mol/mol). (k) HAADF-STEM images and (l) EDS maps of SiO$_2$@MnO$_x$(KMnO$_4$) with a (KMnO$_4$)/(SiO$_2$) ratio of 0.19 (mol/mol).



Fig. 3 SEM images of SiO$_2$@MnO$_x$(Mn-acetate) with (Mn-acetate)/(SiO$_2$) ratios of (a) 0.12, (b) 0.24, (c) 0.49, (d) 0.73, (e) 0.98, and (f) 1.47 (mol/mol). (g) TEM images and (h) EDS maps of SiO$_2$@MnO$_x$(Mn-acetate) with a (Mn-acetate)/(SiO$_2$) ratio of 0.73 (mol/mol).

(Fig. 5 and S1†). The thickness of the top SiO$_2$ shell was controlled by changing the quantity of tetraethyl orthosilicate (TEOS) precursors that were added to SiO$_2$@MnO$_x$@Na$_2$WO$_4$. Regarding the SiO$_2$@MnO$_x$(KMnO$_4$)@Na$_2$WO$_4$@SiO$_2$ catalyst,

the top shell of SiO$_2$ forms a rough surface, mimicking the surface morphology (Na$_2$WO$_4$ layer) of SiO$_2$@MnO$_x$(KMnO$_4$)@Na$_2$WO$_4$. With increasing concentration of top-shell SiO$_2$, small SiO$_2$ particles (∼100 nm) form, covering the surface of SiO$_2$@MnO$_x$(KMnO$_4$)@Na$_2$WO$_4$. The EDS maps and TEM images indicate the formation of thin SiO$_2$ layers on the surface. Top-shell SiO$_2$ also forms on the surface of the SiO$_2$@MnO$_x$(Mn-acetate)@Na$_2$WO$_4$@SiO$_2$ catalyst. During the Mn-acetate deposition, isolated Mn rods form, which are also coated with SiO$_2$. The EDS maps and TEM images indicate that the deposition of SiO$_2$ insignificantly changes the core–shell structure of SiO$_2$@MnO$_x$(Mn-acetate)@Na$_2$WO$_4$.

### 3.4. OCM using core–shell structures

Core–shell catalysts prepared were used for the OCM (Fig. 6 and Table S1†). The OCM activity of SiO$_2$@MnO$_x$(KMnO$_4$)@Na$_2$WO$_4$@SiO$_2$ was measured and compared with those of SiO$_2$@MnO$_x$(KMnO$_4$)@Na$_2$WO$_4$ without outer SiO$_2$ shell, SiO$_2$@MnO$_x$(Mn-acetate)@Na$_2$WO$_4$@SiO$_2$, and conventional Na$_2$WO$_4$/Mn/SiO$_2$. Although SiO$_2$@MnO$_x$(KMnO$_4$)
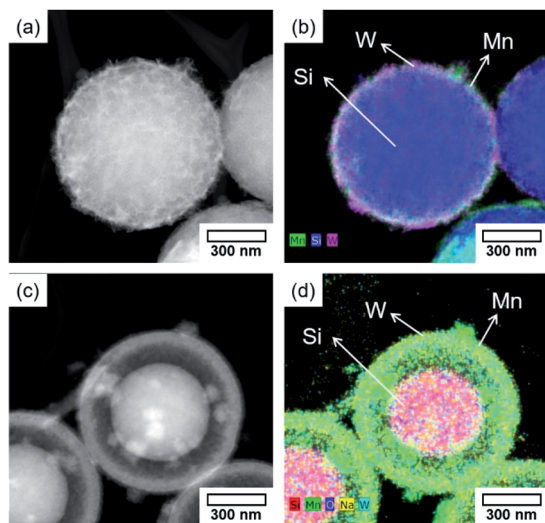
Fig. 4 HAADF-STEM images and EDS maps of (a and b) $SiO_2@$-$MnO_x(KMnO_4)@Na_2WO_4$ and (c and d) $SiO_2@MnO_x(Mn\text{-}acetate)$ $@Na_2WO_4$.

$@Na_2WO_4@SiO_2$ was covered by the outer $SiO_2$ shell, it exhibited the slightly higher $C_{2+}$ selectivity compared to $Na_2WO_4/Mn/SiO_2$ at 740–800 °C. $SiO_2@MnO_x(Mn\text{-}acetate)$ $@Na_2WO_4@SiO_2$ exhibited poor OCM activity with lower $CH_4$ conversion and the lower $C_{2+}$ selectivity which was confirmed by the EDS-STEM images (Fig. 7). $SiO_2@MnO_x(KMnO_4)@Na_2WO_4$ without the outer $SiO_2$ shell also exhibited lower $CH_4$ conversion (4.3–17.0%) compared to $SiO_2@MnO_x(KMnO_4)@Na_2$-$WO_4@SiO_2$ (10.8–25.4%). The higher OCM activity of $SiO_2@MnO_x(KMnO_4)@Na_2WO_4@SiO_2$ compared to that of $SiO_2@MnO_x(KMnO_4)@Na_2WO_4$ without the outer $SiO_2$ shell can be attributed to the better dispersed $Na_2WO_4$ and $MnO_x$ mixed with the outer $SiO_2$ shell as depicted in the EDS-STEM images (Fig. 7). With increasing gas hourly space velocity (GHSV) or decreasing contact time, $CH_4$ conversion decreased, and the $C_{2+}$ selectivity slightly increased (Table S2†). The long term stability of $SiO_2@MnO_x(KMnO_4)@Na_2WO_4@SiO_2$ was also observed, as a stable $C_{2+}$ yield was observed for up to 100 h. That said, the $C_{2+}$ selectivity decreased slightly up to 20 h and remained stable thereafter (Fig. S2†).

The TEM results confirm that core–shell $SiO_2@MnO_x@$-$Na_2WO_4@SiO_2$ catalysts were successfully fabricated (Fig. 1–5). While the use of Mn as an oxygen supplier for the OCM reaction has been suggested,[16] Mn is also required for the production of well-dispersed $Na_2WO_4$ on Mn-based nanosheets in the core–shell structures. The formation of Mn-based nanosheets on the silica core spheres could be clearly observed when the $KMnO_4$ precursor was used. The better catalytic activity of $SiO_2@$-$MnO_x(KMnO_4)@Na_2WO_4@SiO_2$ can be attributed to the deposition of well-dispersed of $Na_2WO_4$ on Mn-based nanosheets. At high OCM reaction temperatures, the core–shell structure of $SiO_2@MnO_x(KMnO_4)@Na_2WO_4@SiO_2$ collapses into a complex $SiO_2$, $MnO_x$, and $Na_2WO_4$ composite. The successful OCM activity of collapsed $SiO_2@MnO_x(KMnO_4)@Na_2WO_4@SiO_2$ can be attributed to the formation of well-dispersed $Na_2WO_4$ particles on the Mn-bearing $SiO_2$ surface, which was derived from
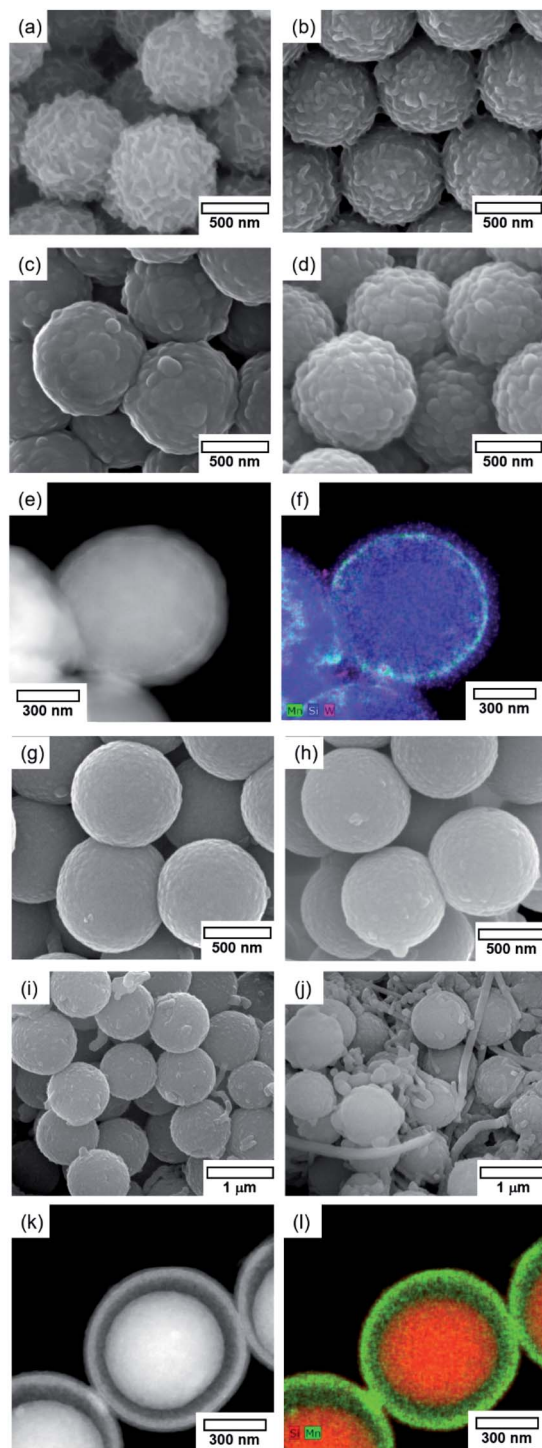


Fig. 5 SEM images of $SiO_2@MnO_x(KMnO_4)@Na_2WO_4@SiO_2$ with ($SiO_2$ core)/($KMnO_4$)/($Na_2WO_4$)/(top-shell $SiO_2$) ratios of (a) 1/2.28/0.01/ 0.03, (b) 1/2.28/0.01/0.07, (c) 1/2.28/0.01/0.14, and (d) 1/2.28/0.01/ 0.29 (in mol) and $SiO_2@MnO_x(Mn\text{-}acetate)@Na_2WO_4@SiO_2$ with ($SiO_2$ core)/(Mn-acetate)/($Na_2WO_4$)/(top-shell $SiO_2$) ratios of (g) 1/0.24/ 0.01/0.03, (h) 1/0.24/0.01/0.07, (i) 1/0.73/0.01/0.14, and (j) 1/1.47/0.01/ 0.29 (in mol). HAADF-STEM images and EDS maps of (e and f) $SiO_2@MnO_x(KMnO_4)@Na_2WO_4@SiO_2$ and (k and l) $SiO_2@MnO_x(Mn\text{-}acetate)@Na_2WO_4@SiO_2$.
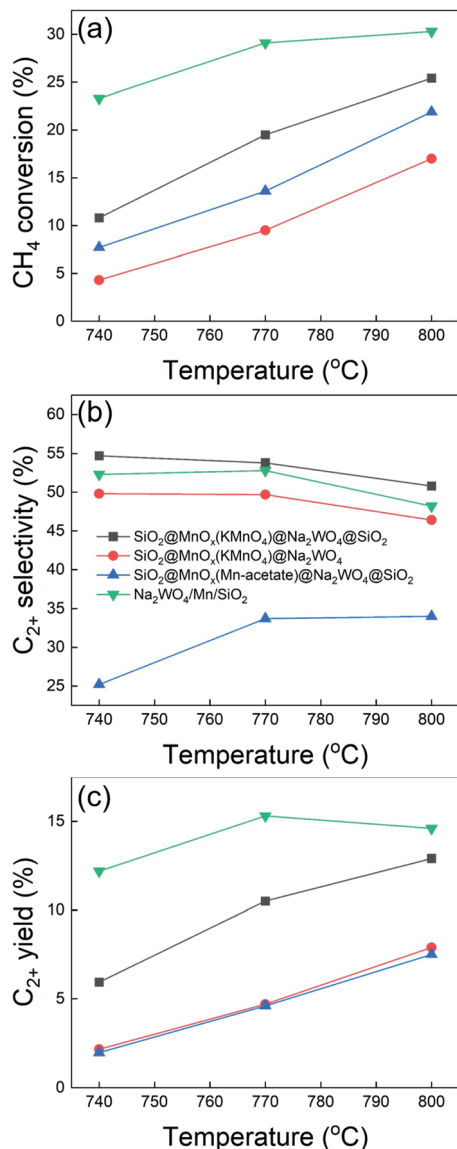
Fig. 6 Results of oxidative coupling of methane using core–shell catalysts. GHSV = 20 000 h$^{-1}$, CH$_4$/O$_2$/N$_2$ = 3/1/1 mol/mol/mol.



Fig. 7 HAADF-STEM images and EDS maps of (a) Na$_2$WO$_4$/Mn/SiO$_2$, (b) SiO$_2$@MnO$_x$(KMnO$_4$)@Na$_2$WO$_4$@SiO$_2$, and (c) SiO$_2$@MnO$_x$(Mn-acetate)@Na$_2$WO$_4$@SiO$_2$ after the OCM reaction.
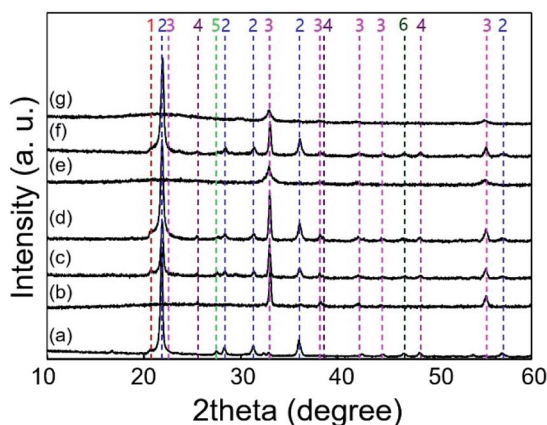


Fig. 8 XRD results of (a) Na$_2$WO$_4$/Mn/SiO$_2$, (b) SiO$_2$@MnO$_x$(KMnO$_4$), (c) SiO$_2$@MnO$_x$(KMnO$_4$)@Na$_2$WO$_4$, (d) SiO$_2$@MnO$_x$(KMnO$_4$)@Na$_2$-WO$_4$@SiO$_2$, (e) SiO$_2$@MnO$_x$(Mn-acetate), (f) SiO$_2$@MnO$_x$(Mn-acetate)@Na$_2$WO$_4$, and (g) SiO$_2$@MnO$_x$(Mn-acetate)@Na$_2$WO$_4$@SiO$_2$. All catalysts were fresh prior to the reaction. (1: tridymite, 2: α-cristobalite, 3: Mn$_2$O$_3$, 4: MnO$_2$, 5: Na$_2$WO$_4$, 6: NaWO$_3$).

the initial core–shell structure. Core–shell structures and highly disperse catalysts are more selective with respect to the formation of C$_{2+}$ compounds because of the confined Na$_2$WO$_4$ structure. Interestingly, SiO$_2$@MnO$_x$(Mn-acetate)@Na$_2$WO$_4$@-SiO$_2$ exhibited spherical core–shell structures at high reaction temperature, despite being fully covered by the outer SiO$_2$ shell which suppressed the OCM reaction.

The XRD measurements indicate that the formation of α-cristobalite SiO$_2$ was observed for SiO$_2$@MnO$_x$(KMnO$_4$)@Na$_2$-WO$_4$@SiO$_2$ and Na$_2$WO$_4$/Mn/SiO$_2$ but not for SiO$_2$@MnO$_x$(Mn-acetate)@Na$_2$WO$_4$@SiO$_2$ (Fig. 8). Because of the stabilizing effects of α-cristobalite SiO$_2$,[17] the poor OCM activity of SiO$_2$@MnO$_x$(Mn-acetate)@Na$_2$WO$_4$@SiO$_2$ can be attributed to the absence of α-cristobalite SiO$_2$. The formation of α-cristobalite SiO$_2$ for SiO$_2$@MnO$_x$(KMnO$_4$)@Na$_2$WO$_4$@SiO$_2$ indicated the formation of a complex mixture of Na$_2$WO$_4$ and the outer

SiO$_2$ shell because the permeation of Na into SiO$_2$ nucleated the α-cristobalite SiO$_2$.

The XPS exhibited distinct peaks of tungsten (W 4f) and sodium (Na 1s) for SiO$_2$@MnO$_x$(KMnO$_4$)@Na$_2$WO$_4$@SiO$_2$, but not for SiO$_2$@MnO$_x$(Mn-acetate)@Na$_2$WO$_4$@SiO$_2$ (Fig. 9). Because the OCM-active tungsten oxide was not clearly observed on the surface of SiO$_2$@MnO$_x$(Mn-acetate)@Na$_2$WO$_4$@-SiO$_2$,[9,16,31,32] the OCM activity of SiO$_2$@MnO$_x$(Mn-acetate)@Na$_2$WO$_4$@SiO$_2$ was lower than those of other catalysts. These
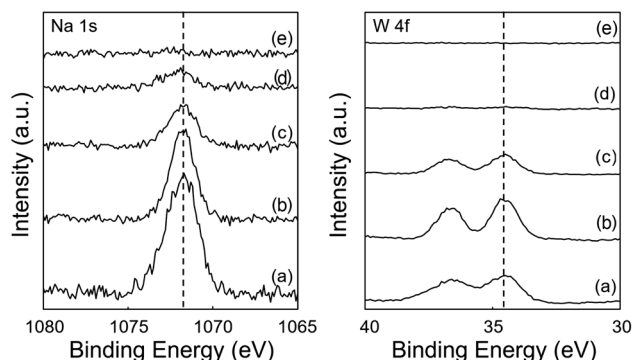
Fig. 9 Na 1s and W 4f XPS results of (a) $Na_2WO_4/Mn/SiO_2$, (b) $SiO_2@MnO_x(KMnO_4)@Na_2WO_4$, (c) $SiO_2@MnO_x(KMnO_4)@Na_2WO_4@SiO_2$, (d) $SiO_2@MnO_x(Mn\text{-}acetate)@Na_2WO_4$, and (e) $SiO_2@MnO_x(Mn\text{-}acetate)@Na_2WO_4@SiO_2$. All catalysts were fresh prior to the reaction.

observations can be attributed to the outer $SiO_2$ shell blocking the active tungsten oxide for $SiO_2@MnO_x(Mn\text{-}acetate)@Na_2WO_4@SiO_2$ as depicted in the EDS-STEM images. $SiO_2@MnO_x(KMnO_4)@Na_2WO_4@SiO_2$ exhibited appreciable W 4f peaks indicating exposed active sites for the OCM.

### 3.5. Reaction mechanism on the core–shell catalysts

$SiO_2@MnO_x(KMnO_4)@Na_2WO_4@SiO_2$ exhibited slightly higher $C_{2+}$ selectivity compared to the conventional $Na_2WO_4/Mn/SiO_2$ catalyst although it was covered by the outer $SiO_2$ shell. The selective OCM activity can be attributed to the formation of a complex of $Na_2WO_4$, $MnO_x$, and $SiO_2$ as observed on the TEM, XRD, and Raman results. The presence of complex mixed oxides improved the dispersion of $Na_2WO_4$ in the mixture of $MnO_x$ and $SiO_2$ selectively catalysing OCM.

## 4. Conclusion

In this study, $SiO_2@MnO_x@Na_2WO_4@SiO_2$ core–shell structures were prepared. Nanostructured shells of Mn oxide and $Na_2WO_4$ consecutively formed and were protected using $SiO_2$ sols. Although the complex core–shell structures were destroyed at a temperature of 700–800 °C at which the OCM to olefins and paraffins was performed, highly dispersed $Na_2WO_4$ on the $MnO_x$ layer is derived from nanoscopic core–shell structures. The $Na_2WO_4$ may be confined to the complex structures of $MnO_x$ and $SiO_2$. The catalyst derived from the core–shell $Na_2WO_4$–Mn–$SiO_2$ complex exhibits an improved production of $C_{2+}$ compounds and the further oxidation of $C_{2+}$ compounds to CO and $CO_2$ may be suppressed by highly dispersed $Na_2WO_4$.

## Conflicts of interest

There are no conflicts to declare.

## Acknowledgements

## Notes and references

1 R. T. Yunarti, S. Gu, J.-W. Choi, J. Jae, D. J. Suh and J.-M. Ha, *ACS Sustainable Chem. Eng.*, 2017, **5**, 3667–3674.

2 C. Hammond, S. Conrad and I. Hermans, *ChemSusChem*, 2012, **5**, 1668–1686.

3 H. R. Godini, S. Xiao, S. Jašo, S. Stünkel, D. Salerno, N. X. Son, S. Song and G. Wozny, *Fuel Process. Technol.*, 2013, **106**, 684–694.

4 Z. Zakaria and S. K. Kamarudin, *Renewable Sustainable Energy Rev.*, 2016, **65**, 250–261.

5 V. Paunović and J. Pérez-Ramírez, *Catal. Sci. Technol.*, 2019, **9**, 4515–4530.

6 Y. Gambo, A. A. Jalil, S. Triwahyono and A. A. Abdulrasheed, *J. Ind. Eng. Chem.*, 2018, **59**, 218–229.

7 T. Ito and J. H. Lunsford, *Nature*, 1985, **314**, 721–722.

8 G. E. Keller and M. M. Bhasin, *J. Catal.*, 1982, **73**, 9–19.

9 S. Arndt, T. Otremba, U. Simon, M. Yildiz, H. Schubert and R. Schomäcker, *Appl. Catal., A*, 2012, **425–426**, 53–61.

10 T. W. Elkins, B. Neumann, M. Bäumer and H. E. Hagelin-Weaver, *ACS Catal.*, 2014, **4**, 1972–1990.

11 G. Lee, I. Kim, I. Yang, J.-M. Ha, H. B. Na and J. C. Jung, *Appl. Surf. Sci.*, 2018, **429**, 55–61.

12 S. Lim, J.-W. Choi, D. J. Suh, K. H. Song, H. C. Ham and J.-M. Ha, *J. Catal.*, 2019, **375**, 478–492.

13 T. W. Elkins and H. E. Hagelin-Weaver, *Appl. Catal., A*, 2013, **454**, 100–114.

14 J. W. Xu, Y. Zhang, Y. M. Liu, X. Z. Fang, X. L. Xu, W. M. Liu, R. Y. Zheng and X. Wang, *Eur. J. Inorg. Chem.*, 2019, 183–194.

15 X. Fang, S. Li, J. Lin and Y. Chu, *J. Mol. Catal.*, 1992, **6**, 427–433.

16 S. Gu, H.-S. Oh, J.-W. Choi, D. J. Suh, J. Jae, J. Choi and J.-M. Ha, *Appl. Catal., A*, 2018, **562**, 114–119.

17 Z. C. Jiang, C. J. Yu, X. P. Fang, S. B. Li and H. L. Wang, *J. Phys. Chem.*, 1993, **97**, 12870–12875.

18 N. S. Hayek, G. J. Khlief, F. Horani and O. M. Gazit, *J. Catal.*, 2019, **376**, 25–31.

19 N. Hiyoshi and T. Ikeda, *Fuel Process. Technol.*, 2015, **133**, 29–34.

20 M. Yildiz, Y. Aksu, U. Simon, T. Otremba, K. Kailasam, C. Gobel, F. Girgsdies, O. Gorke, F. Rosowski, A. Thomas, R. Schomacker and S. Arndt, *Appl. Catal., A*, 2016, **525**, 168–179.

21 D. Sun, S. Wageh, A. A. Al-Ghamdi, Y. Le, J. Yu and C. Jiang, *Appl. Surf. Sci.*, 2019, **466**, 301–308.

22 Y.-F. Huang, X.-Y. Sun, S.-H. Huo, Y. Li and C. Zhong, *Appl. Surf. Sci.*, 2019, **466**, 637–646.

23 J. Y. Lee, W. Jeon, J.-W. Choi, Y.-W. Suh, J.-M. Ha, D. J. Suh and Y.-K. Park, *Fuel*, 2013, **106**, 851–857.

24 W. Stöber, A. Fink and E. Bohn, *J. Colloid Interface Sci.*, 1968, **26**, 62–69.

25 W. Li and D. Zhao, *Adv. Mater.*, 2013, **25**, 142–149.

26 X. Jiang, Y. Wang and M. Li, *Sci. Rep.*, 2014, **4**, 6070.

27 H. Shi, D. Shi, L. Yin, Z. Yang, S. Luan, J. Gao, J. Zha, J. Yin and R. K. Li, *Nanoscale*, 2014, **6**, 13748–13753.

28 D. Yuan, T. Zhang, Q. Guo, F. Qiu, D. Yang and Z. Ou, *Chem. Eng. J.*, 2017, **327**, 539–547.

29 D. Kong, M. Yu, C. Lin, X. Liu, J. Lin and J. Fang, *J. Electrochem. Soc.*, 2005, **152**, H146–H151.

30 M. Qiao, X. Lei, Y. Ma, L. Tian, W. Wang, K. Su and Q. Zhang, *J. Alloys Compd.*, 2017, **693**, 432–439.

31 Y. Kou, B. Zhang, J.-z. Niu, S.-b. Li, H.-l. Wang, T. Tanaka and S. Yoshida, *J. Catal.*, 1998, **173**, 399–408.

32 S.-B. Li, *Chin. J. Chem.*, 2001, **19**, 16–21.